



Pendant bases as proton transfer relays in diiron dithiolate complexes inspired by [Fe–Fe] hydrogenase active site

Zhen Wang^a, Wenfeng Jiang^b, Jianhui Liu^{a,*}, Weina Jiang^a, Yu Wang^a, Björn Åkermark^c, Licheng Sun^{a,d,*}

^a State Key Laboratory of Fine Chemicals, DUT-KTH Joint Education and Research Center on Molecular Devices, Dalian University of Technology (DUT), 158 Zhongshan Road, Box 40, Dalian, Liaoning 116012, PR China

^b Department of Chemistry, Dalian University of Technology (DUT), 110024 Dalian, PR China

^c Department of Organic Chemistry, Arrhenius Laboratory, Stockholm University, 10691 Stockholm, Sweden

^d Department of Chemistry, Organic Chemistry, Royal Institute of Technology (KTH), 10044 Stockholm, Sweden

ARTICLE INFO

Article history:

Received 10 April 2008

Received in revised form 2 June 2008

Accepted 3 June 2008

Available online 7 June 2008

Keywords:

Pendant base

Phosphine ligand exchange

Proton transfer

[Fe–Fe] hydrogenase

ABSTRACT

Three dinuclear iron complexes containing pendant nitrogen bases in phosphine ligands with general formula $(\mu\text{-pdt}) [\text{Fe}_2(\text{CO})_5\text{L}]$ (where pdt is $\text{SCH}_2\text{CH}_2\text{CH}_2\text{S}$, $\text{L} = \text{PPh}_2\text{NH}(\text{CH}_2)_2\text{N}(\text{CH}_3)_2$ (**5**), $\text{PPh}_2\text{NH}(\text{2-NH}_2\text{C}_6\text{H}_4)$ (**6**), $\text{PPh}_2[2\text{-N}(\text{CH}_3)_2\text{CH}_2\text{C}_6\text{H}_4]$ (**7**)), were prepared as the models of the [Fe–Fe] hydrogenase active site. The molecular structures of **5–7** were characterized by X-ray crystallography. The secondary amine in **6** has weak intramolecular hydrogen bonding with both the terminal nitrogen and sulfur atom, which may suggest a proton transfer pathway from amine in phosphine ligand to the sulfur atom of active site. Protonation of complexes **5** and **6** only occurred at the terminal nitrogen atom. Electrochemical properties of the complexes were studied in the presence of triflic acid by cyclic voltammetry.

© 2008 Published by Elsevier B.V.

1. Introduction

The Fe–Fe hydrogenases, the more efficient enzymes in hydrogen production than other types of hydrogenases, have inspired chemists in the bioinorganic community to synthesize close mimics of their active sites in the search for hydrogen production catalysts. The latest spectroscopic, crystallographic and theoretical studies suggest that the active sites consist of bimetallic iron complexes bridged by a 1,3-azadithiolate ligand (Fig. 1) [1–5], although the nature of the bridging ligand could not be solved from X-ray data of the enzymes. DFT calculations have shown that the amine functionality in this dithiolate is the potential position for protonation, which provides a low energy pathway for hydrogen evolution in the natural system [4]. Based on these significant research findings, the structural and functional models of the Fe–Fe hydrogenases active site have been intensively studied in recent years [6–8]. There have been some reports regarding the synthesis and electrochemistry of azadithiolate diiron derivatives $(\mu\text{-SCH}_2)_2\text{NR} [\text{Fe}_2(\text{CO})_6]$ ($\text{R} = \text{H}$, $-\text{CH}_3$, $4\text{-NO}_2\text{C}_6\text{H}_4$, $4\text{-BrC}_6\text{H}_4\text{CH}_2$, $2\text{-BrC}_6\text{H}_4$, $2\text{-CH}_2\text{C}_4\text{H}_3\text{O}$) [9–16]. However, the distance between the nitrogen atom in the dithiolated chelate and the iron atom of the active site is comparatively changeless.

Other experimental and theoretical studies of these model complexes also indicate that bridging hydride may be involved in the catalytic cycle of hydrogenase enzymes and there are other possible pathways as the proton transfer relays that do not require a nitrogen of the azadithiolate ligand [17–20].

Studies on organometallic complexes have shown that pendant nitrogen bases play an important role in proton/hydride exchange reactions [21–23]. An understanding of proton transfer process will be necessary for developing efficient hydrogen production/hydrogen oxidation catalysts. Recently, DuBois and co-workers reported that trans Fe(II) complexes containing the diphosphine ligand with a pendant nitrogen base as the potential model of the iron–iron hydrogenase enzymes can be successively protonated in two steps using increasingly strong acids and a nitrogen atom in a six-membered chelate ring can promote very rapid intra- and intermolecular proton/hydride exchange in octahedral Fe(II) PNP complexes and function as a proton relay for oxidized Fe(III) hydrides as well [24]. Incorporating good donor ligands (cyanide, tertiary phosphines and isonitrile) to the propanedithiolato-bridged dinuclear complex $[(\mu\text{-pdt})\text{Fe}_2(\text{CO})_6]$ (**1**) that bears remarkable structural similarities with the active site of Fe–Fe hydrogenase renders the iron atoms more electron-rich and more protophilic [17,25–28]. These results promoted us to study the role of a pendant base of phosphine ligand in proton/hydride exchange in diiron complexes. In this paper, we report the preparation of three phosphine ligands containing pendant nitrogen bases, and their monosubstituted (5),

* Corresponding authors. Address: State Key Laboratory of Fine Chemicals, DUT-KTH Joint Education and Research Center on Molecular Devices, Dalian University of Technology (DUT), 158 Zhongshan Road, Box 40, Dalian, Liaoning 116012, PR China. Tel.: +86 411 88993886; fax: +86 411 83072185 (J. Liu).

E-mail address: liujh@dlut.edu.cn (J. Liu).

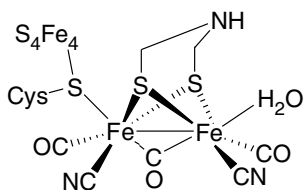


Fig. 1. The H_{ox} state of the Fe-only hydrogenase.

$PPh_2NH(2-NH_2C_6H_4)$ (**6**), $PPh_2[2-N(CH_3)_2CH_2C_6H_4]$ (**7**) by the CO-ligand exchange reaction (see structures in Chart 1). The nitrogen atom of the phosphine ligand in complexes **5–7** can adopt the position closer to the catalytically active site in space than that of the azadithiolated bridgehead in the complexes $(\mu-SCH_2)_2NR[Fe_2(CO)_6]$. As desired, the protonation of the basic nitrogen atom instead of Fe–Fe bond has been observed in the presence of triflic acid.

2. Results and discussion

2.1. Synthesis and spectroscopic characterization

The monosubstituted $2Fe_2S$ complex $(\mu-pdt)[Fe_2(CO)_5PMe_3]$ was chosen as the substrate in our initial studies, based on the consideration that the ligand PMe_3 can increase the electron-density of Fe atom. However, we were unable to obtain the disubstituted products via intermolecular CO-displacement by the phosphine ligand **2–4** in the presence of CO-removing reagent Me_3NO or in refluxing toluene. Therefore we turned our attention to all carbonyl substrate **1**, hoping to obtain monosubstituted $2Fe_2S$ complexes **5–7** and to study the role of a pendant base of phosphine ligand in proton transfer process. By treatment with $Me_3NO \cdot 2H_2O$ as decarbonylation reagent, we obtained the monosubstituted complexes in yield 55–61% (Scheme 1), which is similar to that of PPh_3 monosubstituted complex [29]. All of the three complexes **5–7**, are air and thermally stable in the solid state.

The products obtained were characterized by IR, 1H and ^{31}P NMR spectroscopy and elemental analysis. Their IR data of $\nu(CO)$

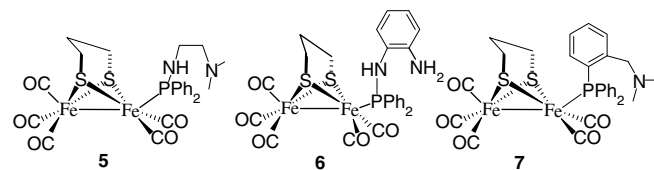


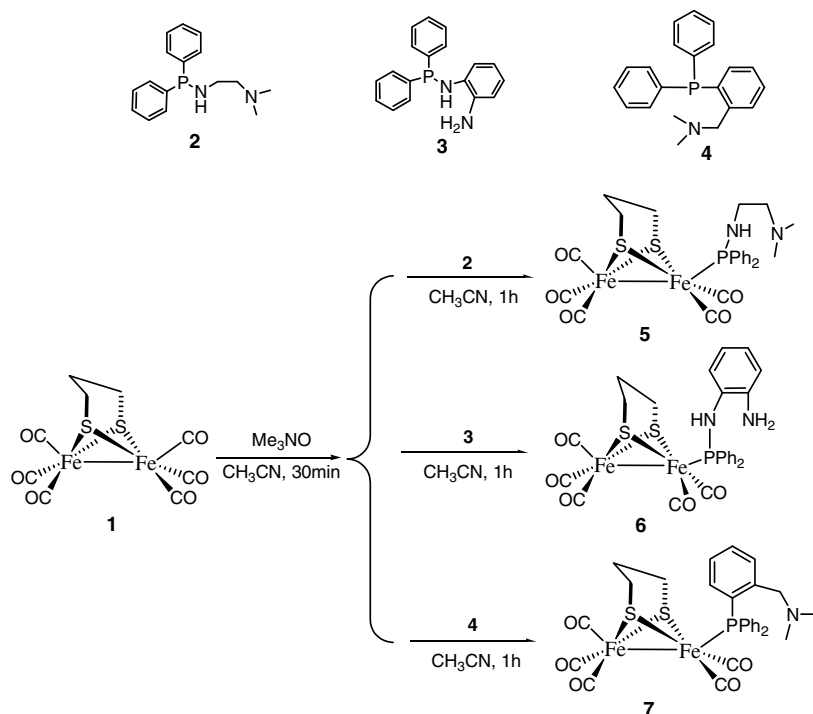
Chart 1. The structures of complexes **5**, **6** and **7**.

are listed in Table 1. Each complex shows three bands in the $\nu(CO)$ stretching region ($1890\text{--}2080\text{ cm}^{-1}$), the same as that of complex $(\mu-pdt)[Fe_2(CO)_5PPh_3]$ [29]. In comparison to all carbonyl complex **1**, the average value of the bands for monosubstituted complex **5–7** are lowered by 50, 52 and 49 cm^{-1} , respectively. It indicates that the electron-donating capability of phosphine ligands **2–4** is similar.

2.2. Molecular structures of complexes **5–7**

The crystallographic structures of **5–7**, which are depicted as solvate-free forms and given as an ORTEP diagram in Fig. 2, belong to the $P2(1)/n$, $Pbca$ and $P2(1)/c$ space groups, respectively. Selected bond lengths and bond angles are listed in Table 2. The Fe_2S_2 skeleton of **5–7** has the well-known butterfly structure found in related diiron complexes $(\mu-SR)_2[Fe_2(CO)_{6-n}L_n]$ [25–29]. Each iron center displays approximately square-pyramidal coordination geometry. The Fe–Fe distances in **5** (2.5029(8) Å), **6** (2.5010(10) Å) and **7** (2.5267(18) Å) are somewhat different compared to the structural data of Fe–Fe bonds (2.5103(11) Å) of complex **1** [29]. Both ^{31}P NMR and X-ray crystallographic analyses of **5–7** suggest that one CO-displacement by tertiary phosphine in **1** affords only an apical isomer, as shown in Fig. 2.

The angles of C(6)–S(1)–Fe(1) [$114.8(2)^\circ$] and C(8)–S(2)–Fe(1) [$114.7(2)^\circ$] in **6** are a little wider than the corresponding angles of C(6)–S(1)–Fe(2) [$111.0(2)^\circ$] and C(8)–S(2)–Fe(2) [$111.6(2)^\circ$]. It shows that the six-membered ring of the propanedithiolate in **6** is pushed away from the site occupied by an apical phosphine



Scheme 1. The synthetic procedure of complexes **5–7**.

Table 1
The IR data of complexes **1**, **5**–**7**

Complex	$\nu(\text{CO})$ (cm^{-1})		
1	2073	2032	1989
5	2053	1974	1928
6	2041	1979	1919
7	2046	1981	1930

ligand, leading to the lean of the propanedithiolate ring towards the $\text{Fe}(\text{CO})_3$ site, as its analogue (μ -pdt) $[\text{Fe}_2(\text{CO})_5\text{PPh}_3]$ [29]. The compounds **5** and **7** show a similar structure feature. The angle of $\text{P}-\text{Fe}(1)-\text{Fe}(2)$ for **5** is 3.66° wider than that of $\text{C}(3)-\text{Fe}(2)-\text{Fe}(1)$ for **7**. However, the difference of corresponding two angles is only $1.52(33)^\circ$ and $0.51(31)^\circ$ for **5** and **6**, respectively. The $\text{Fe}-\text{P}$ bond lengths of $2.2160(13)$ Å in **5**, $2.2139(14)$ Å in **6** and $2.269(2)$ Å in **7** are similar to the values of $\text{Fe}-\text{P}$ bond lengths reported for PR_3 coordinating diiron complexes [29]. The average $\text{Fe}(2)-\text{C}(\text{CO})$ bonds, $1.796(6)$ – $1.772(7)$ Å for **5**–**7**, are slightly shorter than those in **1** [av. $1.800(3)$ Å], and the average $\text{Fe}(1)-\text{C}(\text{CO})$ distance [$1.757(9)$ Å] of **5**–**7** is considerably shortened by ca. 0.022 – 0.032 Å after coordination of phosphine to $\text{Fe}(1)$. Another notable fact is that the $\text{Fe}-\text{C}$ bond lengths in apical positions are decreased in the monosubstituted complexes. A reasonable explanation is that the displacement of CO by the electron-donating phosphine ligand increases the electron-density on one of the iron centers of the diiron dithiolate complex, to give stronger back donation to the CO ligands and weaken the CO bonds.

In the crystalline solid state of complex **5**, the chain $\text{N}(1)-\text{C}(21)-\text{C}(22)-\text{N}(2)$ takes the gauche form. The nonbonding $\text{N}(1)\cdots\text{N}(2)$ distance (2.781 Å) for **5** is apparently shorter than the

sum of the van der Waals radii for two nitrogen atoms (3.0 Å), therefore it easily forms the stable $\text{N}-\text{H}\cdots\text{N}$ intramolecular hydrogen bond. As shown in Fig. 2b, a particularly attractive aspect is that the hydrogen atom of $\text{N}(1)$ has weak intramolecular hydrogen bond with both $\text{N}(2)$ and sulfur atom. The distances and angles of the two kinds of H-bonds in the crystals of complex **6** are given in Table 3. The two intramolecular hydrogen bond might suggest a proton transfer pathway from amine of phosphine ligand to the sulfur atom of active site. Although the $\text{S}\cdots\text{H}$ distance for the intramolecular is longer than that of typically sulfur hydrogen bond [30,31], it may influence the skeleton of $2\text{Fe}_2\text{S}$ whose distance (3.049 Å) of non-bonded two sulfur atoms for **6** is slightly longer than that of two sulfur atoms for **5** (3.03 Å) and for **7** (3.042 Å).

2.3. Protonation of model complexes **5** and **6**

Protonation of **5** and **6** to form corresponding 5H^+ and 6H^+ protonated species occurs in an acetonitrile solution upon addition of triflic acid. The ^1H NMR spectra monitor the protonation processes (Figs. 3 and 4). As 4 equiv. of triflic acid were added to the CD_3CN solution of **5**, the signal of $\text{N}(\text{CH}_3)_2$ at δ 2.09 ppm shifts to δ 2.60 ppm, and the signal of $\text{N}(\text{CH}_2)_2\text{N}$ at 2.24 and 2.74 ppm shift to δ 2.87 and 3.10 ppm, respectively, whereas the peak of the secondary amine, the two phenyl and propanedithiolate bridge have no changes. All of these features indicate the protonation only occurred at terminal tertiary amine. This was also verified by IR. The $\nu(\text{CO})$ band pattern of the protonated derivative for **5** is identical to that of compound **1** with the $\nu(\text{CO})$ values shifting by only 5 cm^{-1} on average. The smaller shift is consistent with ligand-based protonation as expected for the exposed tertiary nitrogen atoms on the phosphine ligand [17].

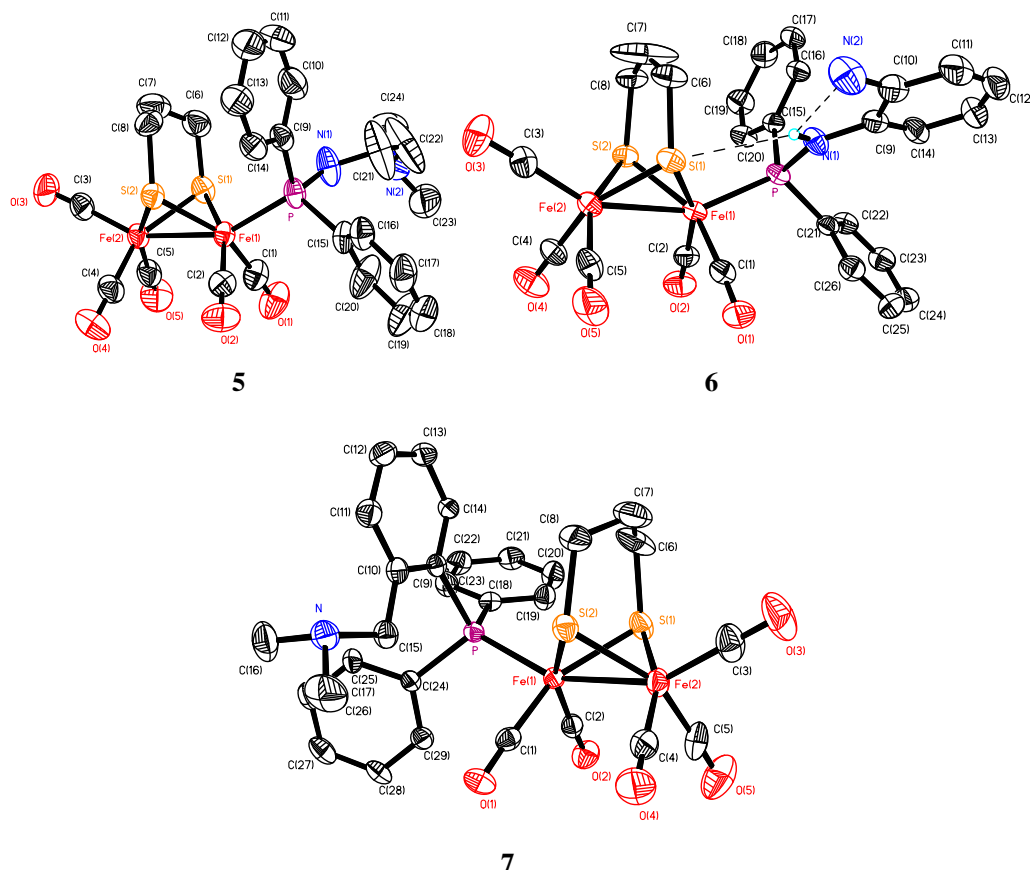


Fig. 2. ORTEP (ellipsoids at 30% probability level) view of **5**, **6** and **7**.

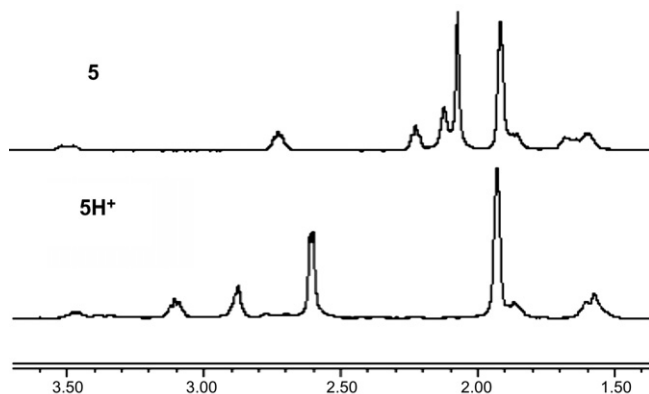
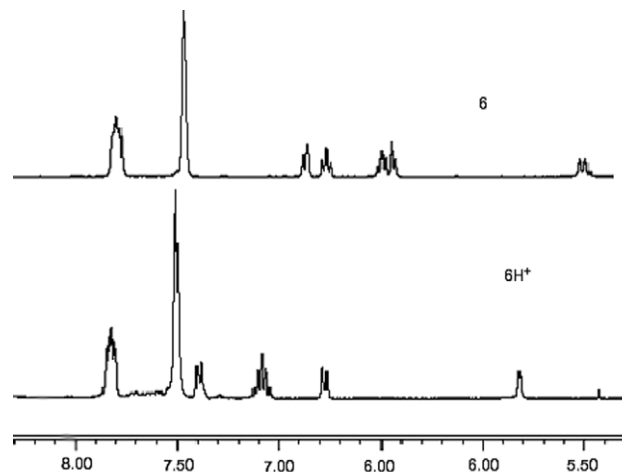
Table 2
Selected bond lengths (Å) and angles (°) for **5–7**

Complex	5	6	7
Bond lengths			
Fe(1)–Fe(2)	2.5029(8)	2.5010(10)	2.5267(18)
Fe(1)–S(1)	2.2532(14)	2.2603(14)	2.269(2)
Fe(1)–S(2)	2.2482(13)	2.2650(15)	2.279(3)
Fe(2)–S(1)	2.2757(14)	2.2673(15)	2.266(3)
Fe(2)–S(2)	2.2550(13)	2.2653(14)	2.269(3)
Fe(1)–P	2.2160(13)	2.2139(14)	2.269(2)
Fe(1)–C(1)	1.755(6)	1.766(6)	1.776(8)
Fe(1)–C(2)	1.764(6)	1.766(6)	1.767(10)
Fe(2)–C(3)	1.796(6)	1.778(6)	1.778(10)
Fe(2)–C(4)	1.772(7)	1.785(6)	1.779(10)
Fe(2)–C(5)	1.778(7)	1.781(6)	1.793(12)
P–N(1)	1.653(5)	1.684(4)	
Bond angles			
P–Fe(1)–S(1)	104.49(5)	103.60(5)	109.23(9)
P–Fe(1)–S(2)	106.59(5)	108.13(5)	105.71(9)
P–Fe(1)–C(1)	97.42(18)	97.28(17)	95.7(2)
P–Fe(1)–C(2)	94.13(17)	97.09(18)	96.7(2)
S(1)–Fe(1)–C(1)	87.55(19)	88.34(17)	155.0(2)
S(1)–Fe(1)–C(2)	161.20(17)	159.22(18)	86.8(2)
S(2)–Fe(1)–C(1)	155.91(18)	154.56(17)	88.0(3)
S(2)–Fe(1)–C(2)	87.65(17)	87.02(17)	157.5(2)
S(1)–Fe(1)–Fe(2)	56.88(4)	56.60(4)	56.09(7)
S(2)–Fe(1)–Fe(2)	56.36(3)	56.50(4)	56.07(7)
S(1)–Fe(2)–C(3)	108.6(2)	105.16(18)	102.3(3)
S(1)–Fe(2)–C(4)	151.9(2)	157.60(19)	159.9(3)
S(1)–Fe(2)–C(5)	86.79(19)	86.92(18)	88.3(3)
S(2)–Fe(2)–C(3)	102.00(18)	105.75(19)	107.4(3)
S(2)–Fe(2)–C(4)	87.23(18)	87.84(17)	87.3(3)
S(2)–Fe(2)–C(5)	158.8(2)	155.19(19)	152.6(3)

Table 3
Distances (Å) and angles (°) for the H-bonds in the crystals of **6**

H-bond	$d_{D...A}$	$d_{H...A}$	D...H–A angle
N(2)···H–N(1)	2.709	2.263	112.30
S(1)···H–N(1)	3.460	2.799	134.81

As 4 equiv. of triflic acid were added to the CD₃CN solution of **6**, the signal of –NC₆H₄N– at δ 6.26 ppm and 6.42 ppm shift to δ 7.39 and 6.77 ppm, respectively, and those at δ 6.76 and 6.47 ppm shift to δ 7.08 ppm. Meanwhile, the signal of –PNH– at 5.47 ppm shift to 5.82 ppm due to the intramolecular hydrogen bond in the two nitrogen atoms. Similar to complex **5**, the protonation for **6** only occurred at terminal nitrogen atom. An excess of triflic acid was needed, and the behavior in the ¹H NMR is the same. In the case of complexes **5** and **6**, no peaks at $\delta < 0$ exist, also showing that the protonation occurred on the N atom rather than to form μ -H

**Fig. 3.** The ¹H NMR spectra of complexes **5** and **5H⁺**.**Fig. 4.** The ¹H NMR spectra of complexes **6** and **6H⁺**.

complex. The $\nu(\text{CO})$ value of the protonated derivative **6H⁺** are shifted by only 6 cm⁻¹ on average. Due to the extremely poor solubility of complex **7** in MeCN, we were unfortunately unable to study its protonation.

2.4. Electrochemistry of model complexes **5–7**

In order to get an estimate of the capability to catalyze hydrogen production, cyclic voltammetry (CV) of the complexes **5**, **6** and **7** (Fig. 5) was performed. Compared with the electrochemical data of the analogous complexes $(\mu\text{-pdt})\{\text{Fe}_2(\text{CO})_5\text{L}\}$ (L = PPh₃, PMe₂Ph, PMe₃) [29], the reductive peaks at the range of –1.8 to –1.9 V are ascribed to the one-electron process Fe^(I)Fe^{(I)/Fe⁽⁰⁾Fe^(I), and the oxidation peaks at the range of 0.6–0.8 V versus Fc/Fc⁺ are assigned to the Fe^(I)Fe^{(I)/Fe^(II)Fe^(I) process [13,32,33]. In the cyclic voltammograms of **5** and **6**, the oxidation peaks at 0.348 V and 0.259 V, which is not observed in the cyclic voltammogram of **7**, is presumably due to the oxidation of the NH group of **5** and **6**. According to the literature [13], the oxidative peak of the NH₂ group of **6** is covered by the peak at 0.259 V. Compared to the all carbonyl complex **1** ($E_{\text{red}} = -1.67$ V vs. Fc/Fc⁺) [14], the first reductive potential is shifted towards more negative potential by 194, 179 and 173 mV for **5–7**, respectively. The core iron atom of complex **5** is harder to reduce due to the better electron-donating capability of ligand **2**.}}

The catalytic proton reduction by compound **5** and **6** was studied through cyclic voltammetry (Fig. 6) on addition of CF₃SO₃H in CH₃CN, with the concentration of 0–10 mM. With the increasing amount of the acid, the first reduction peak of **5** is shifted by around 172 mV towards more positive potential by the addition of excess triflic acid. The reductive peak at –1.702 V corresponds to a one-electron reduction of the protonated complex to **5H⁺**. The reduction current increases and the position of this peak shifts to a more negative potential with increasing concentration of the acid added. Compound **6** show a similar behavior in the CH₃CN solution in the presence of triflic acid (see Fig. 6b). Both of these features seemed indicative of catalytic proton reduction, but a cyclic voltammogram of blank solution indicate that they are not efficient catalysts for the H₂ production (complex **5** showing only minor catalytic ability while complex **6** with no such ability, see Supplemental material). This unfavorable catalytic ability may be attributed to the far distance of the protonated terminal amino groups to the Fe–Fe center of the model compounds of **5** and **6**.

As described above, phosphine ligand containing pendant nitrogen bases in [2Fe₂S] complexes could affect the reduction potential

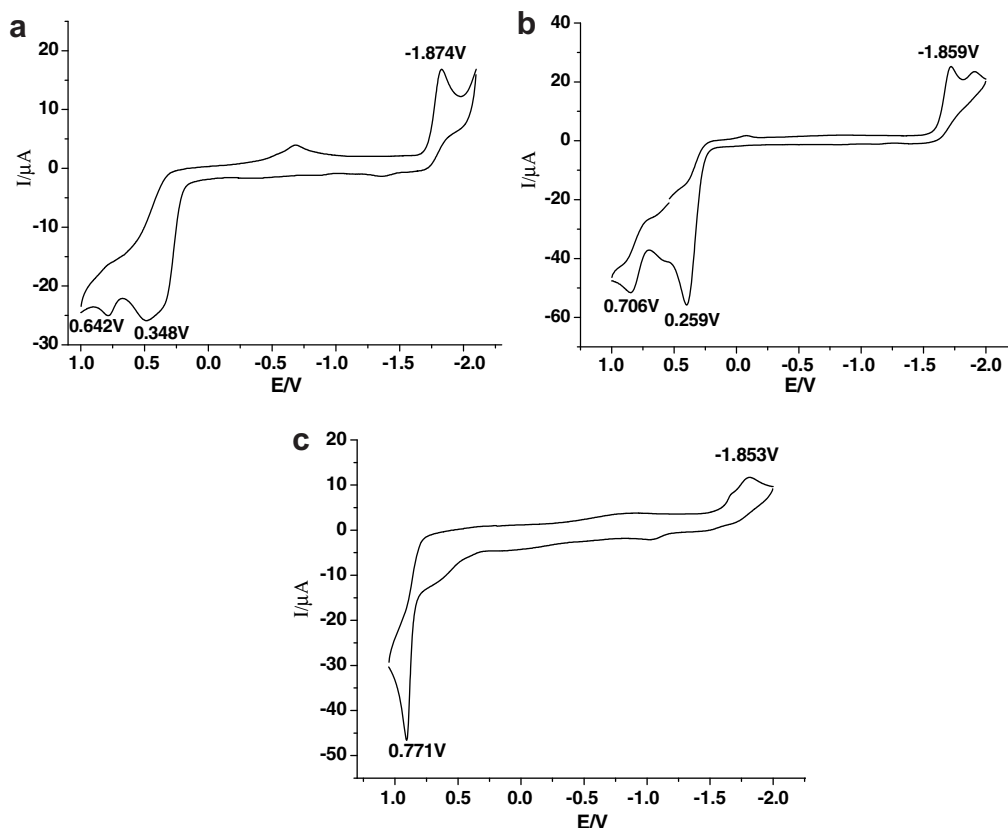


Fig. 5. Cyclic voltammogram of **5** (a), **6** (b) and **7** (c) (1.0 mM) in 0.05 M *n*-Bu₄NPF₆/CH₃CN at a scan rate of 100 mV/s. Potentials are vs. Fc/Fc⁺.

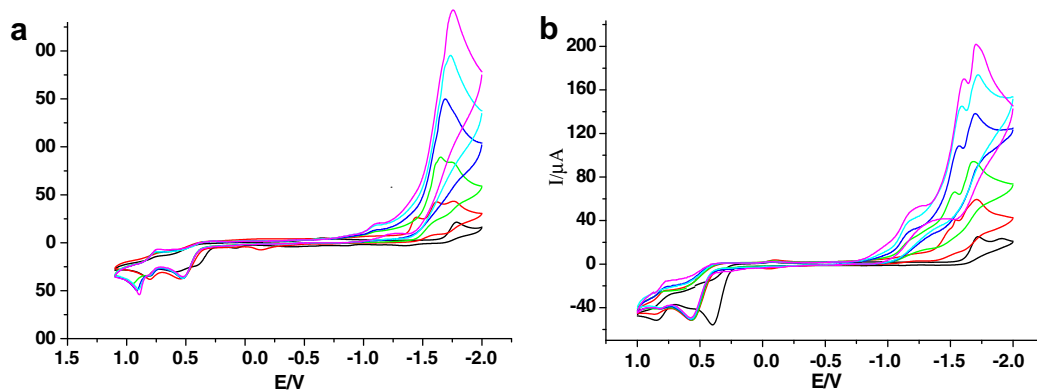


Fig. 6. Cyclic voltammograms of **5** (a) and **6** (b) in CH₃CN in the presence of triflic acid (0, 2, 4, 6, 8, 10 equiv.).

of the iron complexes but the catalytic ability for the proton reduction still need to improve. Further work is focusing on the ligand design with a pendant amine that can closely approach to the Fe–Fe center to form a powerful catalytic center for the H₂ production.

3. Experimental

3.1. Reagents and instruments

All manipulations related to organometallic complexes were performed under dry, oxygen-free nitrogen gas with standard Schlenk techniques. All solvents were purified according to standard meth-

ods. Commercially available chemicals, including 1,3-propanedithiol, diphenylchlorophosphine, dimethylethylenediamine, *o*-diaminobenzene, 2-methyl-*N,N*-dimethylaniline, and Fe(CO)₅, were used without further purification. Starting compounds [(μ-pdt)Fe₂(CO)₆] (**1**) [29,32], *N,N*-dimethyl-*N*-diphenylphosphinoethylenediamine (**2**) [33], *N*-diphenylphosphino-*o*-diaminobenzene (**3**) and *N,N*-dimethyl-*o*-diphenylphosphinobenzylamine (**4**) [34] were prepared according to literature methods. All other reagents were used as purchased without further purification. ¹H and ³¹P NMR spectra were recorded on a Varian INOVA 400 spectrometer. IR spectra were recorded from KBr pellets with a JASCO FT/IR430. Elemental analyses were performed with a Thermoquest-Flash EA 1112 elemental analyzer.

3.2. Procedures

3.2.1. $(\mu\text{-pdt})[\text{Fe}_2(\text{CO})_5\text{PPh}_2\text{NH}(\text{CH}_2)_2\text{N}(\text{CH}_3)_2]$ (**5**)

To the red solution of hexacarbonyldiiron dithiolate **1** (0.97 g, 0.25 mmol) in CH_3CN (15 mL) was added $\text{Me}_3\text{NO} \cdot 2\text{H}_2\text{O}$ (111 mg, 0.1 mmol). When the color of the solution turned dark red, compound **2** (136 mg, 0.5 mmol) was added to the reaction solution. The reaction mixture was stirred for 0.5 h and the color turned red. After the solvent was removed in vacuum, the crude product was purified by column chromatography on neutral Al_2O_3 with $\text{CH}_2\text{Cl}_2/\text{hexane}$ (2:1) as eluent to give **5** as red solid (96 mg, 61%). The crystal suitable for X-ray analysis was obtained from a solution of CH_2Cl_2 in hexane atmosphere at 2 °C. ^1H NMR (CDCl_3) δ 7.65–7.70 (m, 4H, Ph), 7.40 (s, 6H, Ph), 3.33–3.37 (m, 1H, PNHC), 2.72–7.72 (m, 2H, NCH_2C), 2.26 (s, 2H, NCH_2C), 2.12 (s, 6H, NCH_3), 1.84–1.92 (m, 2H, SCH_2C), 1.66–1.70 (m, 2H, SCH_2C), 1.60–1.63 (m, 2H, CCH_2C), ^{31}P NMR (CDCl_3) δ 100.06; IR (KBr): $\nu(\text{CO})$ 2053, 1974, 1928 cm^{-1} . Anal. Calc. for $\text{C}_{24}\text{H}_{27}\text{Fe}_2\text{N}_2\text{O}_5\text{PS}_2$: C, 45.74; H, 4.32; N, 4.44. Found: C, 45.76; H, 4.29; N, 4.59%.

3.2.2. $(\mu\text{-pdt})[\text{Fe}_2(\text{CO})_5\text{PPh}_2\text{NH}(2\text{-NH}_2\text{C}_6\text{H}_4)]$ (**6**)

Complex **6** was prepared by a procedure similar to that of **5**. To the red solution of hexacarbonyldiiron dithiolate **1** (0.97 g, 0.25 mmol) in CH_3CN (15 mL) was added $\text{Me}_3\text{NO} \cdot 2\text{H}_2\text{O}$ (111 mg, 0.1 mmol). When the color of the solution turned dark red, compound **3** (159 mg, 0.5 mmol) was added to the reaction solution. The reaction mixture was stirred for 0.5 h and the color turned red. After the solvent was removed in vacuum, the crude product was purified by column chromatography on silica gel with $\text{CH}_2\text{Cl}_2/\text{hexane}$ (2:1) as eluent to give **6** as red solid (89 mg, 55%). The crystal suitable for X-ray analysis was obtained from a solution of hexane/ CH_2Cl_2 (1/10) at 2 °C. ^1H NMR (CDCl_3) δ 7.77 (s, 4H, Ph), 7.41 (s, 6H, Ph), 6.71 (s, 2H, Ph), 6.41 (t, 1H, Ph, $J = 7.2$ Hz), 6.34 (d, 1H, Ph, $J = 2$ Hz), 5.25 (d, 1H, $J = 15.6$ Hz, PNHPh), 3.46 (s, 2H, PhNH_2), 1.95 (s, 2H, SCH_2C), 1.65 (s, 4H, SCH_2C , CCH_2C), ^{31}P NMR (CDCl_3) δ 96.80; IR (KBr): $\nu(\text{CO})$ 2041, 1979, 1919 cm^{-1} . Anal. Calc.

for $\text{C}_{26}\text{H}_{23}\text{Fe}_2\text{N}_2\text{O}_5\text{PS}_2$: C, 48.02; H, 3.57; N, 4.31. Found: C, 48.23; H, 3.82; N, 4.70%.

3.2.3. $(\mu\text{-pdt})\{\text{Fe}_2(\text{CO})_5\text{PPh}_2[2\text{-N}(\text{CH}_3)_2\text{CH}_2\text{C}_6\text{H}_4]\}$ (**7**)

Complex **7** was prepared by a procedure similar to that of **5**. To the red solution of hexacarbonyldiiron dithiolate **1** (0.97 g, 0.25 mmol) in CH_3CN (15 mL) was added $\text{Me}_3\text{NO} \cdot 2\text{H}_2\text{O}$ (111 mg, 0.1 mmol). When the color of the solution turned dark red, compound **4** (159 mg, 0.5 mmol) was added to the reaction solution. The reaction mixture was stirred for 0.5 h and the color turned red. After the solvent was removed in vacuum, the crude product was purified by column chromatography on silica gel with $\text{CH}_2\text{Cl}_2/\text{hexane}$ (1:5) as eluent to give **7** as red solid (96 mg, 57%). The crystal suitable for X-ray analysis was obtained from a solution of hexane/ CH_2Cl_2 (1/1) at 2 °C. ^1H NMR (CDCl_3) δ 8.00 (s, 1H, Ph), 7.88–7.92 (m, 4H, Ph), 7.59–7.64 (m, 2H, Ph), 7.54 (s, 6H, Ph), 7.34 (t, 1H, Ph, $J = 7.2$ Hz), 3.47 (s, 2H, PhCH_2N), 3.46 (s, 2H, PhNH_2), 1.99 (s, 6H, NCH_3), 1.79–1.84 (m, 2H, SCH_2C), 1.48 (s, 1H, SCH_2C), 1.24–1.29 (m, 3H, SCH_2C , CCH_2C), ^{31}P NMR (CDCl_3) δ 62.72; IR (Film): $\nu(\text{CO})$ 2046, 1981, 1930 cm^{-1} . Anal. Calc. for $\text{C}_{29}\text{H}_{28}\text{Fe}_2\text{NO}_5\text{PS}_2$: C, 51.42; H, 4.17; N, 2.07. Found: C, 51.94; H, 3.98; N, 2.31%.

3.3. Crystal structure determinations of complexes **5–7**

The single crystal X-ray diffraction data were collected with a Siemens Smart CCD diffractometer equipped with graphite monochromated $\text{Mo K}\alpha$ radiation ($\lambda = 0.71073$ Å) for **5–7**. Complete crystal data and parameters for data collection and refinement are listed in Table 4. The structure was solved by direct methods and subsequent difference Fourier syntheses, and refined on F^2 against full-matrix least-squares methods by using the SHELXTL-97 program package. All non-hydrogen atoms were refined anisotropically. The hydrogen atoms located by geometrical calculation, but their positions and thermal parameters were fixed during the structure refinement.

Table 4

Crystallographic data and processing parameters for complexes **5–7**

	5	6 · $0.5\text{C}_6\text{H}_{14}$	7 · CH_2Cl_2
Empirical formula	$\text{C}_{24}\text{H}_{27}\text{Fe}_2\text{N}_2\text{O}_5\text{PS}_2$	$\text{C}_{29}\text{H}_{30}\text{Fe}_2\text{N}_2\text{O}_5\text{PS}_2$	$\text{C}_{30}\text{H}_{30}\text{Cl}_2\text{Fe}_2\text{NO}_5\text{PS}_2$
Formula weight	630.27	693.34	762.24
Crystal system	Monoclinic	Orthorhombic	Monoclinic
Space group	$P2(1)/n$	$Pbca$	$P2(1)/c$
a (Å)	9.7103(5)	20.4923(14)	18.168(11)
b (Å)	18.4200(8)	7.9571(5)	9.223(6)
c (Å)	16.5942(7)	37.192(2)	22.164(13)
α (°)	90.00	90.00	90.00
β (°)	104.830(3)	90.00	113.199(16)
γ (°)	90.00	90.00	90.00
Volume (Å ³)	2869.2(2)	6064.6(7)	3414(4)
Z	4	8	4
D_{calc} (Mg/m ³)	1.459	1.519	1.483
$F(000)$	1296	2856	1560
Crystal size (mm)	0.25 × 0.32 × 0.3	0.37 × 0.2 × 0.2	0.2 × 0.15 × 0.22
Range for data collection (°)	2.21–26.08	1.99–22.72	1.89–22.66
Reflections collected	5656	4065	4511
Independent reflections (R_{int})	3996 (0.0351)	3114 (0.0622)	2987 (0.0632)
Completeness to θ	26.08°, 99.6%	22.72°, 99.4%	22.66°, 99.2%
Data/restraints/parameters	5656/30/329	4065/9/370	4511/0/388
Goodness-of-fit on F^2	1.044	1.061	1.024
Final R indices ($I > 2\sigma(I)$)	$R_1 = 0.0544$ $wR_2 = 0.1425$	$R_1 = 0.0468$ $wR_2 = 0.0982$	$R_1 = 0.0632$ $wR_2 = 0.1580$
R indices (all data)	$R_1 = 0.0803$ $wR_2 = 0.1614$	$R_1 = 0.0679$ $wR_2 = 0.1073$	$R_1 = 0.1039$ $wR_2 = 0.1827$
Largest difference in peak and hole ($e \text{ \AA}^{-3}$)	0.600 and -0.582	0.328 and -0.396	1.110 and -1.005

$$(1) R_1 = (\sum ||F_o| - |F_c||) / (\sum |F_o|)$$

$$(2) wR_2 = [\sum w(F_o^2 - F_c^2)^2 / \sum w(F_o^2)^2]^{1/2}$$

3.4. Protonation of complexes 5–6

A small amount of **5** (2–3 mg) was dissolved in CD₃CN (0.5 mL) in an NMR-tube, and then 1 mL of triflic acid were added directly to the solution for in situ ¹H NMR analysis. Complex **6** was protonated in a similar way.

3.5. Crystal data for 5–7

See Table 4.

3.6. Electrochemistry

A solution of 0.05 M of *n*-Bu₄NPF₆ (Fluka, electrochemical grade) in CH₃CN was used as electrolyte, which was degassed by bubbling with dry argon for 10 min before measurement. Electrochemical measurements were recorded using a BAS-100 W electrochemical potentiostat at a scan rate of 100 mV/s. Cyclic voltammograms were obtained in a three-electrode cell under argon. The working electrode was a glassy carbon disc (diameter 3 mm) successively polished with aqueous alumina powder slurry for 10 min. The reference electrode was a non-aqueous Ag/Ag⁺ electrode (0.01 M AgNO₃ in CH₃CN) and the auxiliary electrode was a platinum wire.

Acknowledgments

We are grateful to the Ministry of Science and Technology of China and the Chinese National Natural Science Foundation (Grant No. 20471013, 20633020 and 20672017), the Program of Introducing Talents of discipline to Universities, the Swedish Energy Agency, the K&A Wallenberg Foundation, and the Swedish Research Council for financial supports of this work. This work was also supported by Program for Changjiang Scholars and Innovative Research Team in University (IRT0711).

Appendix A. Supplementary material

CCDC 628139, 624771 and 658987 contain the supplementary crystallographic data for **5**, **6** and **7**. These data can be obtained free of charge from The Cambridge Crystallographic Data Centre via www.ccdc.cam.ac.uk/data_request/cif. Supplementary data associated with this article can be found, in the online version, at [doi:10.1016/j.jorganchem.2008.06.001](https://doi.org/10.1016/j.jorganchem.2008.06.001).

References

- [1] Y. Nicolet, A.L. de Lacey, X. Vernède, V.M. Fernandez, E.C. Hatchikian, J.C. Fontecilla-Camps, *J. Am. Chem. Soc.* 123 (2001) 1596.
- [2] J.W. Peters, W.N. Lanzilotta, B.J. Lemon, L.C. Seefeldt, *Science* 282 (1998) 1853.
- [3] Y. Higuchi, H. Ogata, K. Miki, N. Yasuoka, T. Yagi, *Structure* 7 (1999) 549.
- [4] H.-J. Fan, M.B. Hall, *J. Am. Chem. Soc.* 123 (2001) 3828.
- [5] A. Volbeda, J.C. Fontecilla-Camps, *J. Chem. Soc., Dalton Trans.* 21 (2003) 4030.
- [6] X.-M. Liu, S.K. Ibrahim, C. Tard, C.J. Pickett, *Coord. Chem. Rev.* 249 (2005) 1641.
- [7] I.P. Georgakaki, L.M. Thomson, E.J. Lyon, M.B. Hall, M.Y. Darensbourg, *Coord. Chem. Rev.* 238 (2003) 255.
- [8] T.B. Rauchfuss, *Inorg. Chem.* 43 (2004) 14.
- [9] H.-X. Li, T.B. Rauchfuss, *J. Am. Chem. Soc.* 124 (2002) 726.
- [10] Z. Wang, J.-H. Liu, C.-J. He, S. Jiang, B. Åkermark, L.-C. Sun, *J. Organomet. Chem.* 692 (2007) 5501.
- [11] J.D. Lawrence, H.-X. Li, T.B. Rauchfuss, M.B. Tnard, M. Rohmer, *Angew. Chem., Int. Ed.* 40 (2001) 1768.
- [12] L.-C. Sun, B. Åkermark, S. Ott, *Coord. Chem. Rev.* 249 (2005) 1653.
- [13] T.-B. Liu, M. Wang, Z. Shi, H.-G. Cui, W.-B. Dong, J.-S. Chen, B. Åkermark, L.-C. Sun, *Chem. Eur. J.* 10 (2004) 4474.
- [14] S. Ott, M. Kritikos, B. Åkermark, L.-C. Sun, R. Lomoth, *Angew. Chem., Int. Ed.* 43 (2004) 1006.
- [15] F. Wang, M. Wang, X. Liu, K. Jin, W. Dong, G. Li, B. Åkermark, L. Sun, *Chem. Commun.* 25 (2005) 3221.
- [16] S. Jiang, J.-H. Liu, L.-C. Sun, *Inorg. Chem. Commun.* 9 (2006) 290.
- [17] R. Mejía-Rodríguez, D. Chong, J.H. Reibenspies, M.P. Soriaga, M.Y. Darensbourg, *J. Am. Chem. Soc.* 126 (2004) 12004.
- [18] F. Gloaguen, J.D. Lawrence, T.B. Rauchfuss, M. Benard, M.-M. Rohmer, *Inorg. Chem.* 41 (2002) 6573.
- [19] M. Bruschi, P. Fantucci, L. De Gioia, *Inorg. Chem.* 42 (2003) 4773.
- [20] T. Zhou, Y. Mo, A. Liu, Z. Zhou, K.R. Tsai, *Inorg. Chem.* 43 (2004) 923.
- [21] S. Park, A.J. Lough, R.H. Morris, *Inorg. Chem.* 35 (1996) 3001.
- [22] H.S. Chu, C.P. Lau, K.Y. Wong, W.T. Wong, *Organometallics* 17 (1998) 2768.
- [23] J.A. Ayllon, S.F. Sayers, S. Sabo-Etienne, B. Donnadieu, B. Chaudret, E. Clot, *Organometallics* 18 (1999) 3981.
- [24] R.M. Henry, R.K. Shoemaker, D.L. DuBois, M.R. DuBois, *J. Am. Chem. Soc.* 128 (2006) 3002.
- [25] M. Schmidt, S.M. Contakes, T.B. Rauchfuss, *J. Am. Chem. Soc.* 121 (1999) 9736.
- [26] E.J. Lyon, I.P. Georgakaki, J.H. Reibenspies, M.Y. Darensbourg, *J. Am. Chem. Soc.* 123 (2001) 3268.
- [27] M.M. Hasan, M.B. Hursthouse, S.E. Kabir, K.M.A. Malik, *Polyhedron* 20 (2001) 97.
- [28] J.L. Nehring, D.M. Heinekey, *Inorg. Chem.* 42 (2003) 4288.
- [29] P. Li, M. Wang, C.-J. He, G.-H. Li, X.-Y. Liu, C.-N. Chen, B. Åkermark, L.-C. Sun, *Eur. J. Inorg. Chem.* (2005) 2506.
- [30] K. Baba, T. Okamura, H. Yamamoto, T. Yamamoto, M. Ohama, N. Ueyama, *Inorg. Chem.* 45 (2006) 8365.
- [31] N. Ueyama, T. Okamura, A. Nakamura, *J. Am. Chem. Soc.* 114 (1992) 8129.
- [32] F. Gloaguen, J.D. Lawrence, M. Schmidt, S.R. Wilson, T.B. Rauchfuss, *J. Am. Chem. Soc.* 123 (2001) 12518.
- [33] D. Chong, I.P. Georgakaki, R. Mejía-Rodríguez, J. Sanabria-Chinchilla, M.P. Soriaga, M.Y. Darensbourg, *Dalton Trans.* 21 (2003) 4158.
- [34] L. Brammer, J.C. Mareque Rivas, C.D. Spilling, *J. Organomet. Chem.* 609 (2000) 36.